

Symmetry indicator-free unconventionality, obstructed edge states and Majorana engineering in 1T-PtSe₂ family

Haohao Sheng,^{1,2,*} Yue Xie,^{1,2,*} Quansheng Wu,^{1,2} Hongming Weng,^{1,2}
Xi Dai,³ B. Andrei Bernevig,⁴ Zhong Fang,^{1,2} and Zhijun Wang^{1,2,†}

¹Beijing National Laboratory for Condensed Matter Physics,
and Institute of Physics, Chinese Academy of Sciences, Beijing 100190, China

²University of Chinese Academy of Sciences, Beijing 100049, China

³Department of Physics, Hong Kong University of Science and Technology, Hong Kong 999077, China

⁴Department of Physics, Princeton University, Princeton, New Jersey 08544, USA

Unconventional materials with mismatch between electronic centers and atomic positions can be diagnosed by symmetry eigenvalues at several high-symmetry k points. Their electronic states are decomposed into a sum of elementary band representations (EBRs), but not a sum of atomic valence-electron band representations (ABRs). In this work, we propose a new kind of symmetry indicator-free (SI-free) unconventional insulators, whose unconventionality has no symmetry eigenvalue indication. Instead, it is identified directly by the computed charge centers by using the one-dimensional (1D) Wilson loop method. We demonstrate that 1T-PtSe₂ is an SI-free unconventional insulator, whose unconventional nature originates from orbital hybridization between Pt- d and Se- $p_{x,y}$ states. The SI-free unconventionality widely exists in the members of PtSe₂ family (MX_2 : $M = \text{Ni, Pd, Pt}$; $X = \text{S, Se, Te}$). The obstructed electronic states are obtained on the edges, which exhibit large Rashba splitting. By introducing superconducting proximity and external magnetic field, we propose that the Majorana zero modes (MZM) can be generated on the corners of 1T-PtSe₂ monolayer.

Introduction. Unconventional materials [1, 2], also known as obstructed atomic limit [3–7], have a branch of energy bands being not consistent with ABRs. These unconventional materials usually be of type I with an EBR at an empty site [Fig. 1(a)], and have a characteristic of the mismatch between electronic charge centers and atomic positions. They usually possess obstructed electronic surface/edge states. The unconventional materials have important applications in many fields, such as electrides [1], solid-state hydrogen storage [2], catalysis [8, 9], and superconductivity [10, 11]. Recently, the type II unconventionality is found in phonon spectra, which has an EBR at an atom with non-atomic vibration orbitals [12–14]. However, due to the limitation of symmetry-based band representations, there is also a new kind of unconventional ones that cannot be indicated by symmetry eigenvalues [Fig. 1(b)], which are analogous to the topological insulators with no symmetry indicators (SI).

As a representative of transition metal dichalcogenides, 1T-PtSe₂ shows many excellent characteristics, like high electron mobility [15], helical spin texture [16], unique magnetic ordering [17], and excellent photocatalytic activity [18], etc [19, 20]. Recently, the edge electronic states of PtSe₂ zigzag ribbon have been predicted theoretically [21] and subsequently confirmed experimentally [22]. The PtSe₂ ribbon is demonstrated to grow naturally along the zigzag direction, and the edge states make few-layer PtSe₂ more semi-metallic [22, 23]. However, the formation mechanism of the edge states is still unclear, and its potential application needs to be further explored.

In this work, we propose a new kind of unconventionality, which can not be indicated by symmetry eigenvalues, termed SI-free unconventionality. Based on first-principles calculations, we demonstrate that 1T-PtSe₂ is an SI-free unconventional insulator, whose unconventional nature is attributed to the band hybridization between Pt- d and Se- $p_{x,y}$ states. The obstructed electronic edge states exhibit large Rashba splitting. By introducing superconducting proximity and external magnetic field, the MZM can be generated at the corners.

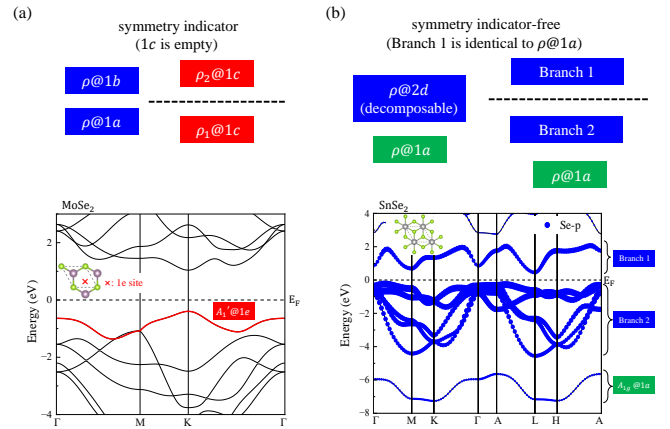


FIG. 1. (Color online) The schematic of the unconventionality of charge mismatch. (a) Those indicated by symmetry eigenvalues at high-symmetry k points only (SI). (b) Those without symmetry indication (SI-free). The SI-free unconventionality is usually found in the compounds with $(\text{Ni/Pd/Pt})^{4+}$, $(\text{Ga/In})^{3+}$, or $(\text{Ge/Sn})^{4+}$ valence states (see Fig. S1).

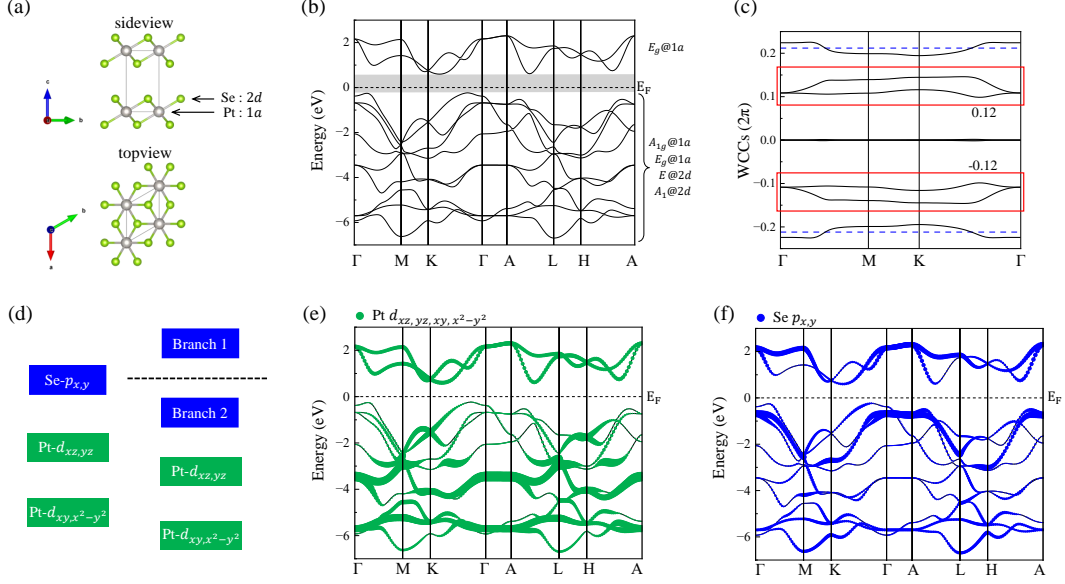


FIG. 2. (Color online) (a) Side and top views of 1T-PtSe₂. The black rectangle represents the unit cell. (b) Band structure and ABRs decomposition of PtSe₂. (c) The z -directed Wannier charge centers (WCCs) for the occupied nine bands. The blue dashed lines (+/-0.21c) indicate the locations of the Se atoms. (d) The schematic of band hybridization, giving rise to the SI-free unconventional nature. (e,f) Orbital-resolved band structures of PtSe₂. The sizes of (e) green and (f) blue circles represent the weights of Pt- d_{xz,yz,xy,x^2-y^2} and Se- $p_{x,y}$ orbitals, respectively.

Electronic band structure and band representation analysis. The 1T-phase PtSe₂ possesses a hexagonal structure with space group $P\bar{3}m1$ (SG #164), where each Pt atom lies at the center of an octahedral cage formed by Se atoms, as shown in Fig. 2(a). The layers are connected by van der Waals force. The Pt and Se atoms are located at the $1a$ and $2d$ Wyckoff positions, respectively. The ABRs of the valence electrons (Pt- d and Se- p) are generated by `pos2ABR` and listed in Table I. The Pt- d orbitals can support two E_g irreducible representations (IrReps). The band structure of PtSe₂ is presented in Fig. 2(b). Based on symmetry eigenvalues (or IrReps), the nine valence bands can be decomposed to the sum of ABRs: $(A_1 + E)@2d + (E_g + A_{1g})@1a$. The two conduction bands belong to $E_g@1a$. It is worth noting that the ABR $E@2d$ is decomposable with one branch identical to $E_g@1a$ (two branches are listed in Table II).

TABLE I. The atomic valence-electron band representations (ABRs) of 1T-PtSe₂. The parameter z of Se is 0.21.

Atom	WKS(q)	Symm. Conf.	Irreps(ρ)	ABRs($\rho@q$)
Pt	$1a$ (000)	$-3m$	$d_{z^2}:A_{1g}$	$A_{1g}@1a$
			$d_{xy,x^2-y^2}:E_g$	$E_g@1a$
			$d_{xz,yz}:E_g$	$E_g@1a$
Se	$2d$ $(\frac{1}{3}\frac{2}{3}z)(\frac{2}{3}\frac{1}{3}-z)$	$3m$	$p_z:A_1$	$A_1@2d$
			$p_{x,y}:E$	$E@2d$

SI-free unconventional nature The ABRs decomposition seems consistent with the valence states of Pt⁴⁺ and Se²⁻, which imply that the Se- p orbitals are fully occupied, and the five Pt- d orbitals are 3/5 filled. The unoccupied bands are supposed to be the two Pt- d orbitals of an E_g IrRep. However, orbital-resolved band structures show large weights of two E_g -IrRep Pt- d orbitals below the Fermi level (E_F) in Fig. 2(e). In contrast, many weights of the E -IrRep Se- p orbitals are above the E_F in Fig. 2(f), which are not consistent with Se²⁻ state. To be precise, by using 1D Wilson loop method, the z -directed Wannier charge centers (WCCs) are obtained, indicating the electronic accurate z -component locations. The $(A_{1g} + E_g)@1a$ bands should have three WCCs at $z = 0c$, while the $(E + A_1)@2d$ bands should have WCCs at $z = \pm 0.21c$, being align with Se positions. The WCCs

TABLE II. The decomposition of the Se- $p_{x,y}$ orbital ABR $E@2d$.

$E@2d$	Branch 1 (identical to $E_g@1a$)	Branch 2
$\Gamma_3^+ \oplus \Gamma_3^-$	Γ_3^+	Γ_3^-
$A_3^+ \oplus A_3^-$	A_3^+	A_3^-
$H_1 \oplus H_2 \oplus H_3$	H_3	$H_1 \oplus H_2$
$K_1 \oplus K_2 \oplus K_3$	K_3	$K_1 \oplus K_2$
$L_1^+ \oplus L_1^- \oplus L_2^+ \oplus L_2^-$	$L_1^+ \oplus L_2^+$	$L_1^- \oplus L_2^-$
$M_1^+ \oplus M_1^- \oplus M_2^+ \oplus M_2^-$	$M_1^+ \oplus M_2^+$	$M_1^- \oplus M_2^-$

for occupied nine bands are obtained in Fig. 2(c), and the results show that the average of the two Wilson bands in the red boxes is $z = 0.12c$, quite away from the Se atoms ($z = 0.21c$; the dashed line). It implies the unconventional nature of charge mismatch in PtSe₂. This SI-free unconventionality is not protected by any symmetry, being of accidental obstructed atomic limit.

To investigate the origin of unconventional nature, we have checked the IrReps (or band hybridization) very carefully. Note only the bands of the same IrReps hybridize. The schematic is given in Fig. 2(d). From the onsite energies of the Wannier-based tight-binding Hamiltonian, the d -orbital $E_g@1a$ is actually lower than $p_{x,y}$ -orbital $E@2d$ at the atomic limit in PtSe₂. Then, the $E@2d$ ($p_{x,y}$ orbitals; Table II) is decomposed into two branches with branch 1 is identical to $E_g@1a$ in terms of IrReps. Due to the hybridization between Pt- d ($E_g@1a$) and Se- $p_{x,y}$ ($E@2d$), branch 1 is unoccupied and branch 2 is fully occupied. This hybridization process gives rise to the SI-free unconventionality, which has to be diagnosed the offset charge centers by using the 1D Wilson loop method. Although it seems that SI-free unconventionality can be removed by changing the relative onsite energy without closing the energy gap, the substitution with the same-group elements usually doesn't qualitatively change the relative onsite energy at all. As a matter of fact, all the 1T- MX_2 compounds of PtSe₂ family (MX_2 ; $M = \text{Ni, Pd, Pt}$; $X = \text{S, Se, Te}$) possess the SI-free unconventionality. First, the onsite energy of M - d orbitals is lower than that of X - $p_{x,y}$ orbitals for all 1T- MX_2 members (extracted from the Wannier90 package). Second, the interlayer hybridization of p_z orbital may lead the metallicity in some 1T- MX_2 compounds, which doesn't really affect the SI-free unconventionality (relying on the $p_{x,y}$ and d orbitals). Recently, the existences of SI-free unconventionality and obstructed hinge states are demonstrated in NiTe₂ bulk, and the magnetic field filtering of hinge supercurrent in NiTe₂-based Josephson junctions is observed experimentally [24].

On the other hand, we find that the SI-free unconventionality due to the band hybridization (inducing the splitting of the decomposable EBR) widely exists in the compounds with (Ga/In)³⁺ or (Ge/Sn)⁴⁺ valence states, which suggest that the s -orbital states are almost empty and above the E_F . The detailed band representation analyses and orbital-resolved band structures are presented for SnSe₂, CuInSe₂, and Cu₂ZnGeSe₄ in Fig. S1. On the contrary, the results show that the s -orbital states are quite far below the E_F . These SI-free unconventional compounds have exhibited superconductivity [25, 26], and optoelectronic or solar cell applications [27, 28] in experiments.

Obstructed edge states. Due to the unconventional nature of the electronic band structure, obstructed edge states are expected. The band dispersions on the zigzag edge [along x axis in Fig. S2(a)] are presented in Fig. 3

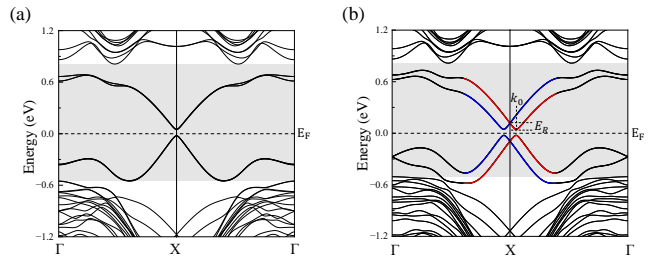


FIG. 3. (Color online) Band structures (a) without and (b) with SOC of PtSe₂ ribbon with zigzag edge. Red and blue bands indicate the different spin channels due to SOC (see Fig. S3 for detail). The k_0 and E_R denote the momentum offset and Rashba energy, respectively. The zigzag-edge state shows an energy of 67 meV.

(The armchair edge states have a relatively large gap in Fig. S4). Neglecting spin-orbit coupling (SOC), the edge states emerge in the bulk band gap ($\sim 1\text{eV}$; shadowed area), as shown in Fig. 3(a). The dispersion of the edge states at X point is like a gapped 1D Dirac cone, rather than a parabolic band, as the linear dispersion survives in a wide range (1/3 of edge BZ). The gap of the edge Dirac cone is 0.07 eV. This result is consistent with the previous theoretical and experimental results [21–23]. Here, we find that SOC can split it into two Dirac cones, exhibiting large Rashba splitting in Fig. 3(b). The coupling strength of the Rashba SOC can be obtained as $\alpha_R = \frac{2E_R}{k_0} = 3.35 \text{ eV}\text{\AA}$, as large as the Bi/Ag(111) surface alloy [29] and BiTeI [30], where $k_0 = 0.043 \text{ \AA}$ and $E_R = 0.072\text{eV}$ denote the momentum offset and Rashba energy, respectively.

Majorana engineering. Due to the existence of 1D edge states with large Rashba splitting, we suggest that the zigzag edge of 1T-PtSe₂ manifests as the 1D semiconducting nanowire [31], which becomes an equivalent spinless p -wave Kitaev chain [32] under superconducting proximity and external magnetic field. Considering the armchair edge of 1T-PtSe₂ monolayer with a large gap, by tuning the chemical potential into the zigzag edge states, the MZM could be generated at the corners of the rectangle sheet of 1T-PtSe₂ monolayer. The MZM was proposed on the corner of the quantum spin Hall with anisotropy [33]. Here, we propose to generate the MZM in the unconventional insulator with different edge states.

To simulate the above, we construct a lattice model (two copied of Bernevig-Hughes-Zhang (BHZ) models), which reads

$$H_{lat}(k_x, k_y) = M(\mathbf{k})\Gamma_{0z0} - \beta \sin k_x (\cos \theta \Gamma_{zxy} + \sin \theta \Gamma_{zxx}) + \beta \sin k_y \Gamma_{0y0} + \xi \Gamma_{z00} - \alpha \Gamma_{xx0} + d \Gamma_{x00}. \quad (1)$$

Here, $M(\mathbf{k}) = M_0 + B(\cos k_x + \cos k_y)$ and $\Gamma_{ijk} = \rho_i \sigma_j s_k$ ($i, j, k = 0, x, y, z$). Pauli matrices ρ act on BHZ, and σ act on orbital subspace and s acts on spin subspace. ξ adds energy difference between the two copies of BHZ

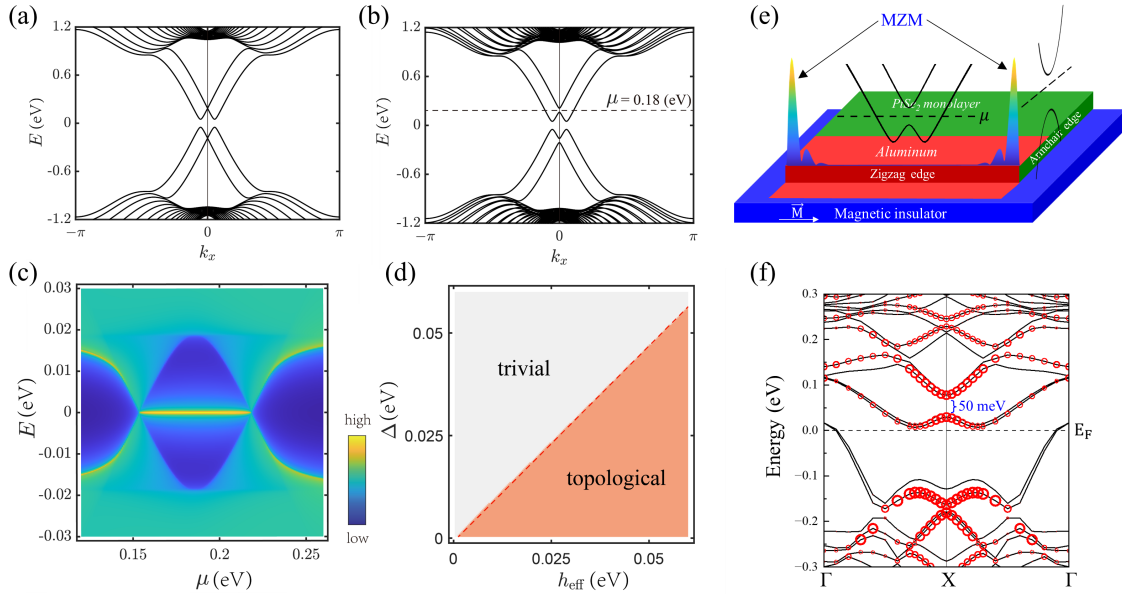


FIG. 4. (Color online) Numerical simulations using the lattice model. (a,b) Energy dispersion in a wire geometry along x periodically with open boundary in y ($L_y = 20$ lattice sites), without (a) and with (b) external magnetic field. In (c), with magnetism ($h_{\text{eff}} = 0.04$) and superconducting pairing ($\Delta = 0.02$), we plot the corner spectrum evolution v.s. chemical potential μ by using the iterative Green function method on the same wire geometry in (a,b). One can see that when tuning the chemical potential inside the magnetic gap, the zero-energy Majorana bound states appear (the bright yellow line in the middle of the surface gap). (d) Phase diagram with superconducting gap v.s. magnetic gap with fixed chemical potential. The red regime holds Majorana end states while the grey regime does not. The parameters are $M_0 = -1.5eV$, $B = 1.5eV$, $\beta = -1.2eV$, $\alpha = 0.05eV$, $\xi = -0.2eV$, $d = 0.3eV$. (e) Schematic diagram for the growth of Majorana nanowire. The zigzag edge hosts the Rashba SOC band structure with a large Zeeman split, but the armchair edge hosts a trivial gapped band structure. (f) Band structure with SOC of PtSe₂ ribbon with zigzag edge on CrGeTe₃ substrate. The magnetic moment of CrGeTe₃ substrate is set parallel to the x direction (along the zigzag edge direction). The size of red circle represents the weight of right edge in PtSe₂ ribbon. The gap opened by Zeeman split is labeled.

edge Dirac states. α mixes the two Dirac states on the edges. d makes the difference at two different edges. As shown in Fig. 4 (a,b), we plot the y -directed (zigzag) edge dispersions without and with magnetic field. Within the magnetic gap ($0.15eV < \mu < 0.22eV$), we demonstrate that superconducting proximity can induce MZM, bounding to the corners, as the other edge has a trivial gapped state. In the end, we obtained the phase diagram in Fig. 4(d).

Finally, we propose that the ferromagnetic insulator CrGeTe₃ is a proper substrate to induce the magnetic gap on the zigzag of 1T-PtSe₂ monolayer. The structure for this simulation is shown in Fig. S2(b). The results of Fig. 4(f) show that the x -directed magnetic moment of CrGeTe₃ substrate can cause a large Zeeman split (50 meV) at X point. Compared by a conventional s -wave BCS superconductor, *e.g.* Aluminum, we suggest that the MZM at the corners of 1T-PtSe₂ monolayer is experimentally accessible.

Discussion. The SI-free unconventional nature of charge mismatch may not have any SI, analogue to SI-free topological insulators. But it can be directly diagnosed by the computed electron charge centers by using the 1D Wilson loop method. It widely exists in nature, such as

1T- MX_2 family. We demonstrate that 1T-PtSe₂ is an SI-free unconventional insulator, whose unconventional nature originates from the band hybridization between Pt- d and Se- $p_{x,y}$ states. The obstructed electronic states on the zigzag edge exhibit large Rashba splitting. Like the superconducting nanowire, these 1D edge state becomes an equivalent spinless p -wave Kitaev chain under superconducting proximity and external magnetic field. With the high mobility and large Zeeman gap on the magnetic substrate CrGeTe₃, the MZM at the corners of 1T-PtSe₂ monolayer is experimentally accessible.

Acknowledgments. This work was supported by the National Natural Science Foundation of China (Grants No. 11974395, No. 12188101), the Strategic Priority Research Program of Chinese Academy of Sciences (Grant No. XDB33000000), National Key R&D Program of Chain (Grant No. 2022YFA1403800), and the Center for Materials Genome.

-
- * These authors contributed equally to this work.
† wzj@iphy.ac.cn
- [1] S. Nie, Y. Qian, J. Gao, Z. Fang, H. Weng, and Z. Wang, *Phys. Rev. B* **103**, 205133 (2021).
 - [2] J. Gao, Y. Qian, H. Jia, Z. Guo, Z. Fang, M. Liu, H. Weng, and Z. Wang, *Science Bulletin* **67**, 598 (2022).
 - [3] Y. Xu, L. Elcoro, G. Li, Z.-D. Song, N. Regnault, Q. Yang, Y. Sun, S. Parkin, C. Felser, and B. A. Bernevig, “Three-dimensional real space invariants, obstructed atomic insulators and a new principle for active catalytic sites,” (2021), [arXiv:2111.02433](https://arxiv.org/abs/2111.02433) [[cond-mat.mtrl-sci](https://arxiv.org/abs/2111.02433)].
 - [4] B. Bradlyn, L. Elcoro, J. Cano, M. Vergniory, Z. Wang, C. Felser, M. I. Aroyo, and B. A. Bernevig, *Nature* **547**, 298 (2017).
 - [5] H. C. Po, H. Watanabe, and A. Vishwanath, *Phys. Rev. Lett.* **121**, 126402 (2018).
 - [6] Z.-D. Song, L. Elcoro, and B. A. Bernevig, *Science* **367**, 794 (2020).
 - [7] Y. Xu, L. Elcoro, Z.-D. Song, M. G. Vergniory, C. Felser, S. S. P. Parkin, N. Regnault, J. L. Mañes, and B. A. Bernevig, “Filling-enforced obstructed atomic insulators,” (2021), [arXiv:2106.10276](https://arxiv.org/abs/2106.10276) [[cond-mat.mtrl-sci](https://arxiv.org/abs/2106.10276)].
 - [8] G. Li, Y. Xu, Z. Song, Q. Yang, Y. Zhang, J. Liu, U. Gupta, V. Süß, Y. Sun, P. Sessi, S. S. P. Parkin, B. A. Bernevig, and C. Felser, *Advanced Materials* **34**, 2201328 (2022).
 - [9] D. Shao, J. Deng, H. Sheng, R. Zhang, H. Weng, Z. Fang, X.-Q. Chen, Y. Sun, and Z. Wang, *Research* **6**, 0042 (2023).
 - [10] H. Wu *et al.*, *Nature* **604**, 653 (2022).
 - [11] Z. Yang, H. Sheng, Z. Guo, R. Zhang, Q. Wu, H. Weng, Z. Fang, and Z. Wang, “Superconductivity in unconventional metals,” (2023), [arXiv:2306.08347](https://arxiv.org/abs/2306.08347) [[cond-mat.mtrl-sci](https://arxiv.org/abs/2306.08347)].
 - [12] R. Zhang, J. Deng, Y. Sun, Z. Fang, Z. Guo, and Z. Wang, “Large shift current, π zak phase and unconventional nature in se and te,” (2022), [arXiv:2211.04116](https://arxiv.org/abs/2211.04116) [[cond-mat.mtrl-sci](https://arxiv.org/abs/2211.04116)].
 - [13] Y. Xu, M. G. Vergniory, D.-S. Ma, J. L. Mañes, Z.-D. Song, B. A. Bernevig, N. Regnault, and L. Elcoro, “Catalogue of topological phonon materials,” (2022), [arXiv:2211.11776](https://arxiv.org/abs/2211.11776) [[cond-mat.mtrl-sci](https://arxiv.org/abs/2211.11776)].
 - [14] R. Zhang, H. Sheng, J. Deng, Z. Yang, and Z. Wang, “Unconventional phonon spectra and obstructed edge phonon modes,” (2023), [arXiv:2305.09453](https://arxiv.org/abs/2305.09453) [[cond-mat.mtrl-sci](https://arxiv.org/abs/2305.09453)].
 - [15] Y. Zhao, J. Qiao, Z. Yu, P. Yu, K. Xu, S. P. Lau, W. Zhou, Z. Liu, X. Wang, W. Ji, and Y. Chai, *Advanced Materials* **29**, 1604230 (2017).
 - [16] W. Yao, E. Wang, H. Huang, K. Deng, M. Yan, K. Zhang, K. Miyamoto, T. Okuda, L. Li, Y. Wang, H. Gao, C. Liu, W. Duan, and S. Zhou, *Nature Communications* **8**, 14216 (2017).
 - [17] A. Avsar, C.-Y. Cheon, M. Pizzochero, M. Tripathi, A. Ciarrocchi, O. V. Yazyev, and A. Kis, *Nature Communications* **11**, 4806 (2020).
 - [18] W. Yeliang, L. Linfei, Y. Wei, S. Shiru, S. J. T., P. Jinbo, R. Xiao, L. Chen, O. Eiji, W. Yu-Qi, W. Eryin, S. Yan, Z. Y. Y., Y. Hai-tao, S. Eike F., I. Hideaki, S. Kenya, T. Masaki, C. Zhaohua, Z. Shuyun, D. Shixuan, P. Stephen J., S. T. Pantelides, and G. Hong-Jun, *Nano Lett.* **15**, 4013–4018 (2015).
 - [19] K. Zhang, M. Yan, H. Zhang, H. Huang, M. Arita, Z. Sun, W. Duan, Y. Wu, and S. Zhou, *Phys. Rev. B* **96**, 125102 (2017).
 - [20] X. Lin, J. C. Lu, Y. Shao, Y. Y. Zhang, X. Wu, J. B. Pan, L. Gao, S. Y. Zhu, K. Qian, Y. F. Zhang, D. L. Bao, L. F. Li, Y. Q. Wang, Z. L. Liu, J. T. Sun, T. Lei, C. Liu, J. O. Wang, K. Ibrahim, D. N. Leonard, W. Zhou, H. M. Guo, Y. L. Wang, S. X. Du, S. T. Pantelides, and H.-J. Gao, *Nature Materials* **16**, 717 (2017).
 - [21] S. Liu and Z. Liu, *Phys. Chem. Chem. Phys.* **20**, 21441 (2018).
 - [22] H. Wang, Z. Liu, Y. Sun, X. Ping, J. Xu, Y. Ding, H. Hu, D. Xie, and T. Ren, *Nano Research* **15**, 4668 (2022).
 - [23] R. Kempt, A. Kuc, T. Brumme, and T. Heine, “Edge conductivity in ptse₂ nanostructures,” (2023), [arXiv:2306.04365](https://arxiv.org/abs/2306.04365) [[cond-mat.mtrl-sci](https://arxiv.org/abs/2306.04365)].
 - [24] T. Le, R. Zhang, C. Li, R. Jiang, H. Sheng, L. Tu, X. Cao, Z. Lyu, J. Shen, G. Liu, F. Liu, Z. Wang, L. Lu, and F. Qu, “Magnetic field filtering of the hinge supercurrent in unconventional metal nite₂-based josephson junctions,” (2023), [arXiv:2303.05041](https://arxiv.org/abs/2303.05041) [[cond-mat.mes-hall](https://arxiv.org/abs/2303.05041)].
 - [25] E. B. Lochocki, S. Vishwanath, X. Liu, M. Dobrowolska, J. Furdyna, H. G. Xing, and K. M. Shen, *Applied Physics Letters* **114** (2019), [10.1063/1.5084147](https://doi.org/10.1063/1.5084147), 091602.
 - [26] Y. Song, X. Liang, J. Guo, J. Deng, G. Gao, and X. Chen, *Phys. Rev. Mater.* **3**, 054804 (2019).
 - [27] W. Li, Z. Pan, and X. Zhong, *J. Mater. Chem. A* **3**, 1649 (2015).
 - [28] L. Choubrac, M. Bär, X. Kozina, R. Félix, R. G. Wilks, G. Brammertz, S. Levchenko, L. Arzel, N. Barreau, S. Harel, M. Meuris, and B. Vermang, *ACS Applied Energy Materials* **3**, 5830 (2020).
 - [29] C. R. Ast, J. Henk, A. Ernst, L. Moreschini, M. C. Falub, D. Pacilé, P. Bruno, K. Kern, and M. Grioni, *Phys. Rev. Lett.* **98**, 186807 (2007).
 - [30] L. Cai, C. Yu, W. Zhao, Y. Li, H. Feng, H.-A. Zhou, L. Wang, X. Zhang, Y. Zhang, Y. Shi, J. Zhang, L. Yang, and W. Jiang, *Nano Letters* **22**, 7441 (2022), PMID: 36099337.
 - [31] J. Alicea, Y. Oreg, G. Refael, F. von Oppen, and M. P. A. Fisher, *Nature Physics* **7** (2011), [10.1038/nphys1915](https://doi.org/10.1038/nphys1915).
 - [32] A. Y. Kitaev, *Physics-Uspekhi* **44**, 131 (2001).
 - [33] Y.-J. Wu, J. Hou, Y.-M. Li, X.-W. Luo, X. Shi, and C. Zhang, *Phys. Rev. Lett.* **124**, 227001 (2020).
 - [34] P. E. Blöchl, *Phys. Rev. B* **50**, 17953 (1994).
 - [35] G. Kresse and D. Joubert, *Phys. Rev. B* **59**, 1758 (1999).
 - [36] G. Kresse and J. Furthmüller, *Computational Materials Science* **6**, 15 (1996).
 - [37] G. Kresse and J. Furthmüller, *Phys. Rev. B* **54**, 11169 (1996).
 - [38] J. P. Perdew, K. Burke, and M. Ernzerhof, *Phys. Rev. Lett.* **77**, 3865 (1996).
 - [39] J. Gao, Q. Wu, C. Persson, and Z. Wang, *Computer Physics Communications* **261**, 107760 (2021).
 - [40] M. Marzari, A. A. Mostofi, J. R. Yates, I. Souza, and D. Vanderbilt, *Rev. Mod. Phys.* **84**, 1419 (2012).

SUPPLEMENTARY MATERIAL

Calculation and Methodology

We carried out the first-principles calculations based on the density functional theory (DFT) with projector augmented wave (PAW) method [34, 35], as implemented in the Vienna *ab initio* simulation package (VASP) [36, 37]. The generalized gradient approximation (GGA) in the form of Perdew-Burke-Ernzerhof (PBE) function [38] was employed for the exchange-correlation potential. The kinetic energy cutoff for plane wave expansion was set to 450 eV. The Brillouin zone (BZ) was sampled by Monkhorst-Pack method in the self-consistent process, with a $18 \times 18 \times 10$ \mathbf{k} -mesh for PtSe₂ bulk and a $10 \times 1 \times 1$ \mathbf{k} -mesh for PtSe₂ ribbon. The thickness of the vacuum layers along b and c directions were set to > 20 Å for PtSe₂ ribbon. The irreducible representations (IrReps) of electronic states were obtained by the program `IRVSP`. The EBRs/ABRs decomposition of the band structure is done on the `UnconvMat` website with the obtained `tqc.data` [39]. The maximally localized Wannier functions for the Pt- d and Se- p orbitals were constructed by using the Wannier90 package [40].

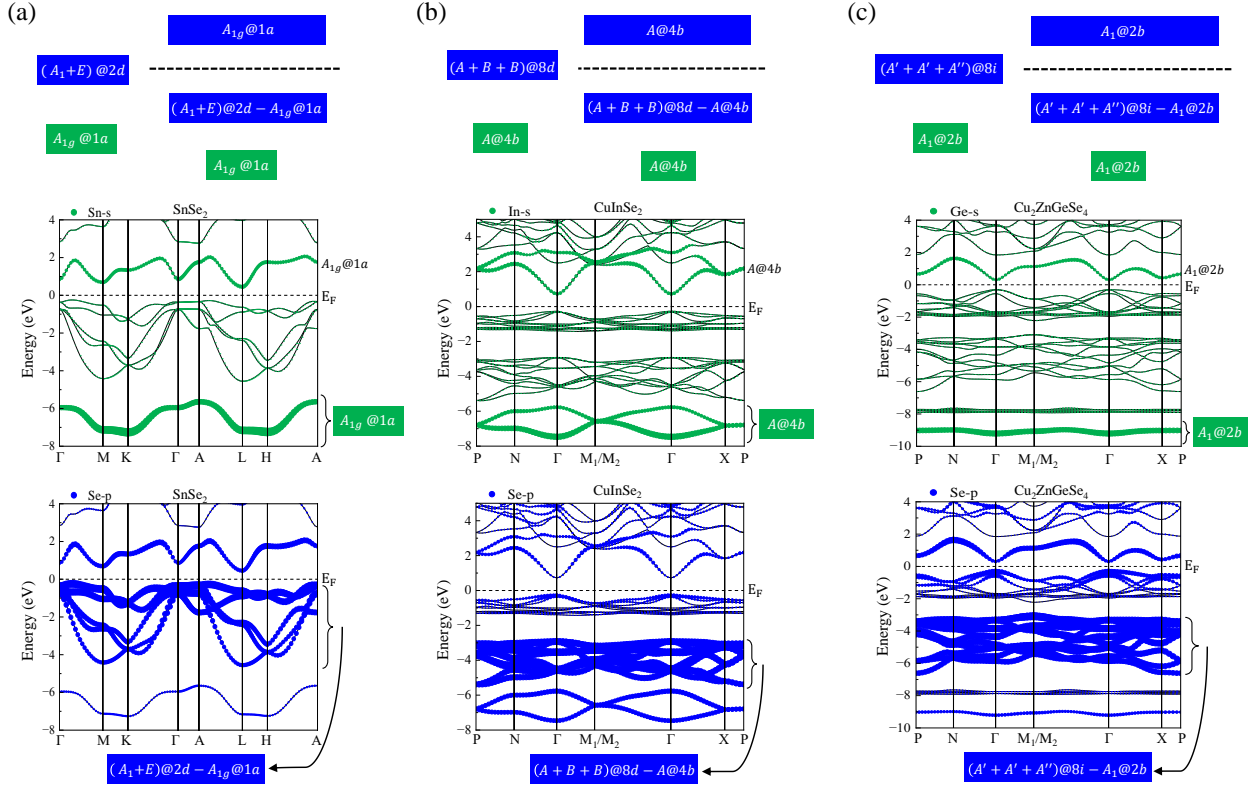


FIG. S1. (Color online) The schematics of band hybridization and orbital-resolved MBJ band structures for (a,b) SnSe₂ (SG #164), (c,d) CuInSe₂ (SG #122), and (e,f) Cu₂ZnGeSe₄ (SG #121). The sizes of green and blue circles represent the weights of corresponding s and p orbitals, respectively.

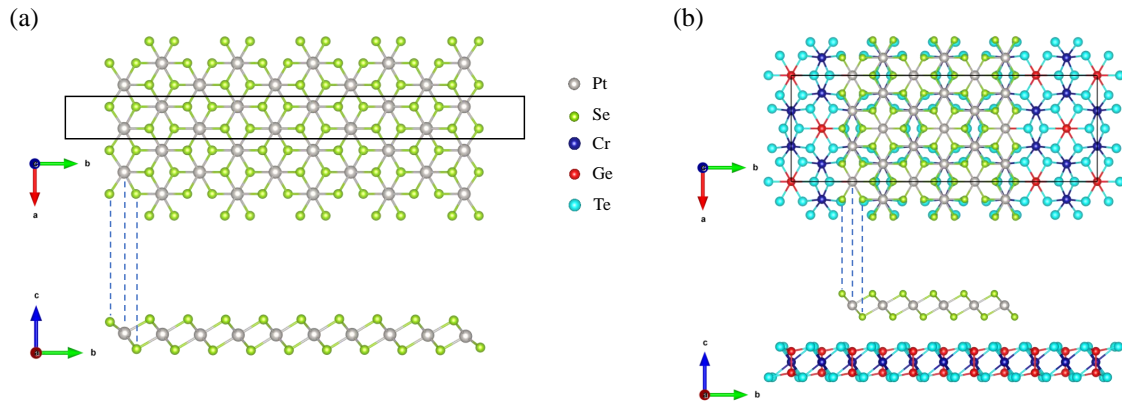


FIG. S2. (Color online) (a) Top and side views of PtSe₂ ribbon with zigzag edge. (b) Top and side views of PtSe₂ ribbon with zigzag edge on CrGeTe₃ substrate. The black rectangle represents the unit cell.

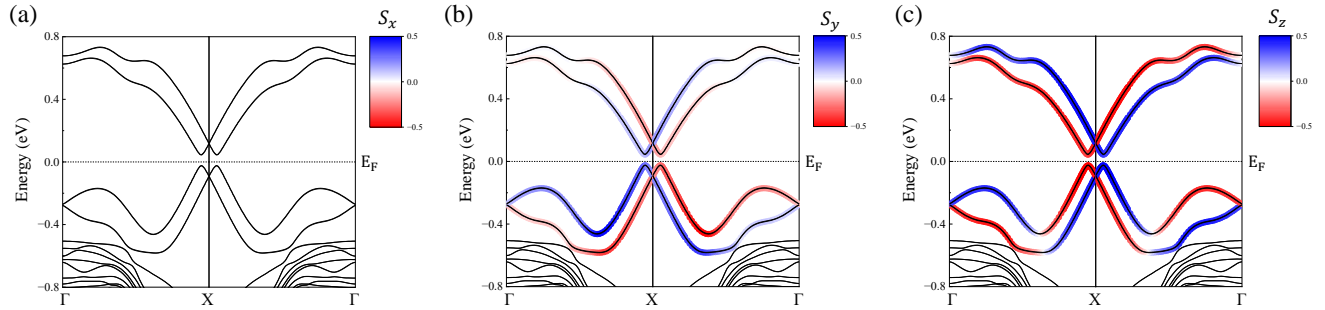


FIG. S3. (Color online) Spin-resolved band structures of PtSe₂ ribbon with zigzag edge, considering SOC. The color scales represent the expectation value of spin components (a) $\langle S_x \rangle$, (b) $\langle S_y \rangle$, and (c) $\langle S_z \rangle$, which are obtained by projecting the contributions from one edge.

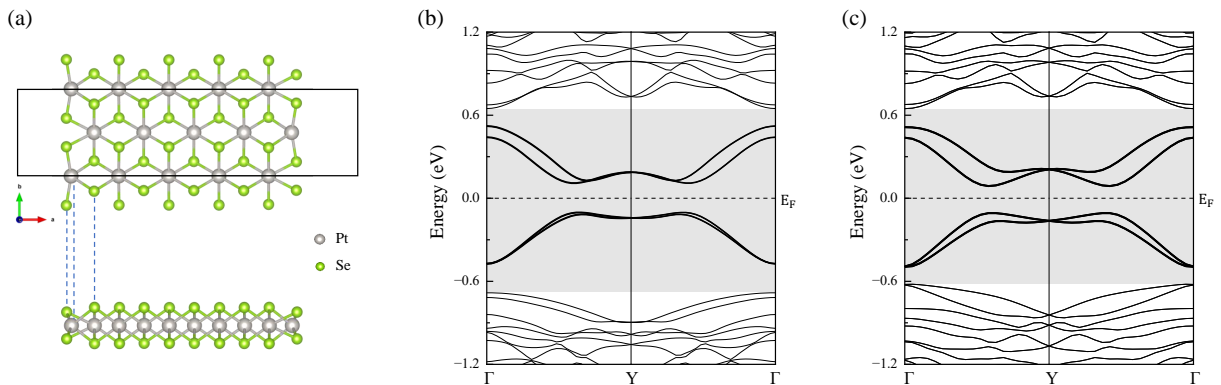


FIG. S4. (Color online) (a) Top and side views of PtSe₂ ribbon with amchair edge. The black rectangle represents the unit cell. Band structures (b) without and (c) with SOC of PtSe₂ ribbon with amchair edge. The amchair-edge state shows an energy of 195 meV.